3. R.B. Waterhouse, S.D. Targonski, and D.M. Kokotoff, Design and performance of small printed antennas, IEEE Trans Antennas Propagat 46 (1998), 1629–1633.
4. R.B. Waterhouse, Small printed antennas with low cross-polarised fields, IEE Electron Lett 33 (1997), 1280–1281.
5. H.K. Kan, D. Pavlickovski, and R.B. Waterhouse, Small dual L-shaped printed antenna, IEE Electron Lett 39 (2003), 1632–1633.
6. D. Pavlickovski and R.B. Waterhouse, Shorted patches mounted on high impedance ground planes, IEEE Int Antennas Propagat Symp., Monterey, CA, 2004, pp. 3601–3604.

INFLUENCE OF POST-TREATMENT CONDITIONS ON PHOTOREACTIVE EFFECT OF Zn:Fe:LiNbO$_3$ CRYSTALS

Shuang-Quan Fang,[1] De-cai Ma,[2] Biao Wang,[1] Fu-Ri Ling,[1] and G. Wang[1]
[1] School of Physics and Engineering
Sun Yat-Sen University
Guangzhou 510275, China
[2] Electro-Optics Technology Center
Harbin Institute of Technology
Harbin 150001, China

Received 15 November 2005

ABSTRACT: *Three kinds of different Zn:Fe:LiNbO$_3$ wafers are prepared by proper reduction or oxidation post-treatment processes. The optical-damage-resistance abilities and photorefractive properties are studied using the optical compensator technique and two-wave coupling measurement, respectively. The holographic storage properties, that is, diffraction efficiency, writing time, erasure time, photorefractive sensitivity, and dynamic range, are also measured or calculated. The analyses indicate that the sample disposed by reduction is the most proper media for holographic storage application.* © 2006 Wiley Periodicals, Inc. Microwave Opt Technol Lett 48: 986–988, 2006; Published online in Wiley InterScience (www.interscience.wiley.com). DOI 10.1002/mop.21542

Key words: *Zn:Fe:LiNbO$_3$; post-treatment; optical damage resistance; photorefractive properties*

1. INTRODUCTION

With their excellent nonlinear optical and photorefractive properties, LiNbO$_3$ crystals have been widely applied in holographic storage, Q-switches, waveguide devices, and optical amplifiers. Fe:LiNbO$_3$ crystal is still one of the preferred media used in volume holographic storage [1, 2], but the long response time [3] and strong light-scattering effect [4] limit its application in practice. For solving this question, the following methods have been adopted: (i) doping optical-damage-resistant impurities such as MgO [4, 5], ZnO [6, 7], In$_2$O$_3$ [8], and Sc$_2$O$_3$ [9]; (ii) changing [Li]/[Nb] ratio [10, 11]; (iii) heating sample to a certain temperature [12]; (iv) proper oxidation or reduction post-treatment process [13, 14].

Proper post-treatment should be responsible for many properties in LiNbO$_3$ crystals. For example, Liu et al. [15] found that the oxidized processing was necessary for the doped LiNbO$_3$ crystals to yield nonvolatile holographic storage and obtained the critical oxidation-reduction state of crystal between volatile and nonvolatile storage [16]. Peithmann et al. [17] investigated small polarons in reduced Fe:LiNbO$_3$ crystals by non-steady-state photocurrent techniques and concluded that the lifetime and influence of the small polarons grew upon reduction. It is well known that valence state of Fe ions and defect distribution in crystals can be changed by proper oxidation or reduction treatment, whereas the photovoltaic current j_{pv} is proportional to [Fe^{2+}] and the photoconductivity σ_{ph} is proportional to [Fe^{2+}]/[Fe^{3+}] ratio [18, 19]. In this paper, the effect of post-treatment on Zn:Fe:LiNbO$_3$ as a kind of holographic recording material is investigated systematically.

TABLE 1 Composition of Raw Material and Sizes of the Samples

Sample	LN–A	LN–O	LN–R
[ZnO] (mol%)	3	3	3
[Fe$_2$O$_3$] (wt.%)	0.03	0.03	0.03
Appearance	Transparent	Transparent	Transparent
Wafer thickness (mm)	4.5	4.5	4.5
Treatment	As grown	Oxidation	Reduction
Growth atmosphere	Air	Air	Air

2. EXPERIMENTAL

2.1. Samples Preparation

The LiNbO$_3$ crystal doped with 0.03 wt.% Fe$_2$O$_3$ and 3.0 mol% ZnO was grown along the *c*-axis from congruent melt using a resistance furnace with an automatic diameter control system based on the Czochralski method. All the raw materials include Li$_2$CO$_3$, Nb$_2$O$_5$, Fe$_2$O$_3$, and ZnO. The compositions of the raw materials and sizes of the samples are given in Table 1. The optimum growth condition, that is, the axial-direction temperature gradient of 40°C/cm, growth rate of 1.5 mm/h, and the rotating rate of 20 rpm, were adopted to grow a high-quality sample. The grown sample was multidomain and had to be polarized before use. The polarizing electric current was 5 mA/cm^2 and the polarizing temperature was 1200°C.

The crystal was sliced into three wafers perpendicular to the *b*-axis, in which one still kept an as-grown state; the others were for oxidation and reduction treatment. The oxidation and reduction post-treatment were performed in an SiC heater furnace using Nb$_2$O$_5$ and Li$_2$CO$_3$ powder, respectively; thus, no other impurities were introduced. The oxidized treatment was performed by embedding the wafer into the Nb$_2$O$_5$ powder and heating the wafer gradually to 1150°C, then annealing after keeping the temperature for 10 h. The reduction treatment was performed by embedding the wafer into the Li$_2$CO$_3$ powder and heating the wafer gradually to 550°C, then annealing after keeping the temperature for 24 h. Finally, all the wafers were polished to a mirror surface on both sides using SiC powders and diamond paste.

2.2. Measurement

The unpolarized light absorption spectra along the *y*-axis for Zn:Fe:LiNbO$_3$ crystals were measured by using CARYIE UV spectrophotometer, which wavelength range is from 300 to 900 nm.

The optical-damage-resistance ability was measured using the optical compensator technique, with a Senarmont compensator [20, 21], in which a weak He–Ne laser (wavelength 6238 Å, intensity 1.0 mW, and diameter 1.5 mm) was used as the probe beam and optical damage is induced with an Ar$^+$ laser (wavelength 4880 Å and diameter 1.5 mm) at an incident power of 300 mW. A photodetector is used to monitor the change in the transmitted He–Ne beam intensity as a function of time.

The photorefractive properties of the samples are obtained by two-wave coupling measurement, as shown in Figure 1. Two

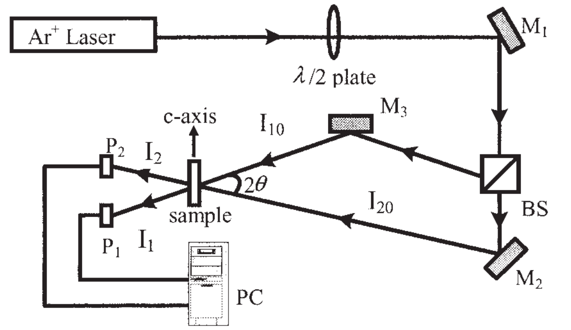

Figure 1 Experimental setup of the two-wave coupling experiment

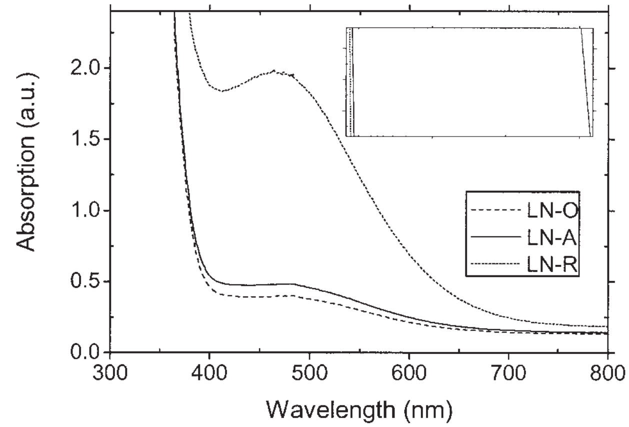

Figure 2 UV absorption spectrum of Zn:Fe:$LiNbO_3$

coherent Ar^+ laser beams (wavelength $\lambda = 5145$ Å) with equal intensity ($I_{10} = I_{20} = 265$ mW/cm^2) irradiate on the sample at grating period $\Lambda = 1.4$ μm in the crystal, in which the c-axis is oriented to be in the incident plane and perpendicular to the bisector of the two beam. The diffraction efficiency η is an important parameter, which can be defined as $\eta = I_2'/(I_2 + I_2') \times 100\%$, where I_2 is the transmitting intensity of I_{20} before the grating is built and I_2' is the diffractive intensity of I_{20} after the grating is built. During the holographic recording process, the diffraction efficiency begins to increase to a maximum value at the writing period; then the diffraction efficiency gradually decays to zero after switches off the writing beam. The recording and erasure process can be approximately described by the following equations. For the recording period,

$$\eta = \eta_0[1 - \exp(-t/\tau_W)]^2. \tag{1}$$

For the erasure period,

$$\eta = \eta_0[\exp(-t/\tau_E)]^2, \tag{2}$$

where τ_W and τ_E are the writing-time and erasure-time constants, respectively, which can be obtained by fitting the experimental curves of diffraction efficiency.

Dynamic range ($M\#$) and sensitivity (S) are two main performances to evaluate the holographic storage properties, which can be expressed as [22]:

$$M\# = \frac{A_0 \tau_E}{\tau_W}, \tag{3}$$

$$S = \frac{(d\sqrt{\eta}/dt)|_{t=0}}{IL} = \frac{A_0/\tau_W}{IL}, \tag{4}$$

where A_0 denotes the saturation hologram strength, expressed as $\sqrt{\eta_0}$.

3. RESULTS AND DISCUSSION

The ultraviolet-visible spectra of Zn:Fe:$LiNbO_3$ crystals under different post-treatment conditions are shown in Figure 2. The reduction treatment makes the absorption edge of the crystal shift to the infrared band, in contrast, the absorption edge shifts to ultraviolet band for oxidation treatment. A visible absorption band center near the 500-nm wavelength is observed and this band increases significantly after reduction treatment.

The relation between the photo-induced birefringence changes ($\delta\triangle n$) of the optical grade Zn:Fe:$LiNbO_3$ crystals after different post-treatment and irradiation time is shown in Figure 3. The saturated birefringence change value of the oxidized sample is the largest and that of the reduced sample is the lowest among three samples. The photoinduced birefringence change in $LiNbO_3$ can be described by the well-known formula $\delta\Delta n \cong Rj_{ph}/\sigma = Rk\alpha I/\sigma$, where j_{ph} is the photovoltaic current, R is the generalized electro-optical coefficient, k is the Glass constant, α is the optical absorption coefficiency, I is the light intensity, and $\sigma = \sigma_d + \sigma_{ph}$, where $\sigma_d \ll \sigma_{ph}$, σ_d is the dark conductivity, and σ_{ph} is the photoconductivity. It is well known that the photovoltaic current is proportional to I and [Fe^{2+}], whereas the photoconductivity in $LiNbO_3$ is proportional to [Fe^{2+}]/[Fe^{3+}] concentration ratio [18, 19, 23], so that the photoinduced birefringence change is proportional to [Fe^{3+}] (I kept constant). Therefore, increasing [Fe^{3+}] for oxidation treatment results in the increasing photoinduced birefringence change, whereas on the contrary, the reduction treatment results in a decreasing photoinduced birefringence change.

The photorefractive properties have been measured or calculated and the results are listed in Table 2. Intense light absorption may be responsible for the low diffraction value in the reduction sample. In addition, the dynamic range of the reduction sample and the photorefractive sensitivity of the oxidation sample are the largest among all the samples. The oxidation and reduction treatments both make the writing or erasure time shorter, but the erasure time of the reduction sample is longer than that of the oxidation sample.

From the above analysis, the reduction sample should be a kind of optimizing photorefractive material among all the samples.

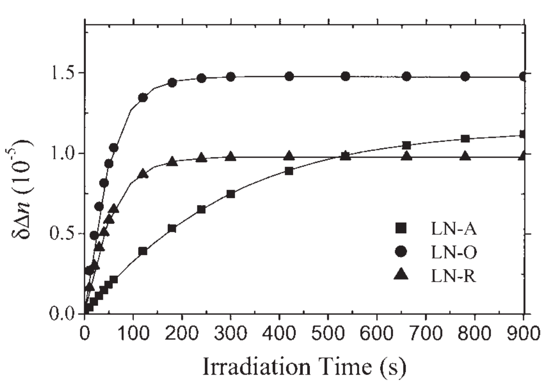

Figure 3 Photo-induced birefringence changes ($\triangle n$) as a function of Ar^+ laser irradiation time in the Zn:Fe:LN crystal for three post-treatment conditions

TABLE 2 Photorefractive Properties of the Zn:Fe:$LiNbO_3$ Crystals with Different Post-Treatment Conditions

	LN–A	LN–O	LN–R
η_0 (%)	23.0	27.2	13.8
τ_W (s)	300	50	55
τ_E (s)	500	112	400
S (cm/J)	0.0134	0.0875	0.0566
$M\#$	0.8	1.2	2.7

4. CONCLUSION

In conclusion, the photorefractive properties of Zn:Fe:$LiNbO_3$ crystals after different post-treatment processes have been investigated. Among all the samples, Zn:Fe:$LiNbO_3$ crystal disposed by reduction presented the lowest photo-induced birefringence change and excellent photorefractive properties; therefore, it is the most proper media for holographic storage application.

ACKNOWLEDGMENT

This work was supported by the National Natural Science Foundation of China (50232030, 10172030), the National Science Foundation of Heilongjiang Province, the Ministry of Science and Technology of China through the High-Tech Program (2001AA31304), and the National Committee of Defense Science and Technology.

REFERENCES

1. P. Boffi, M. Chiara Ubaldi, D. Piccinin, C. Frascolla, and M. Martinelli, IEEE Photon Technol Lett 12 (2000), 1355.
2. G.W. Burr and I. Leyva, Opt Lett 25 (2000), 499.
3. L. Shi, R. Wang, and B. Wang, J Cryst Growth 256 (2003), 103.
4. T. Zhang, B. Wang, F.-R. Ling, S.-Q. Fang, and Y.-H. Xu, Materials Chemistry and Physics 83 (2004), 350.
5. J. Liu, W. Zhang, and G. Zhang, Solid State Commun 98 (1996), 523.
6. T.R. Volk, N. Razumovski, A.V. Mamaev, and N.M. Rubinina, J Opt Soc Am B 13 (1996), 1457.
7. W. Zheng, N. Zhang, L. Zhao, and Y. Xu, Opt Commun 227 (2003), 259.
8. W. Xu, R. Wang, M. Li, and Y. Xu, Proc SPIE 3899 (1999), 468.
9. R. Nevado, E. Camarillo, D. Bravo, I. Aguirre de Carcer, G. Lifante, and F. Jaque, Mater Lett 52 (2002), 1.
10. Y. Furukawa, K. Kitamura, Y. Ji, G. Montemezzani, M. Zgonik, C. Medrano, and P. Gunter, Opt Lett 22 (1997), 501.
11. W. Zheng, C. Zhao, L. Zhao, and Y. Xu, Mater Lett 58 (2004), 326.
12. J. Rams, A. Alcazar-de-Velasco, M. Carrascosa, J.M. Cabrera, and F. Agullo-Lopoz, Opt Commun 178 (2000), 211.
13. H. Hatano, T. Yamaji, S. Tanaka, Y. Furukawa, and K. Kitamura, Jpn J Appl Phys 38 (1999), 1820.
14. X.-J. Chen, D.-S. Zhu, B. Li, T. Ling, and Z.-K. Wu, Opt Lett 28 (2001), 998.
15. Y. Liu, L. Liu, L. Xu, and C. Zhou, Opt Commun 181 (2000), 47.
16. Y. Liu and L. Liu, J Opt Soc Am B 19 (2002), 2413.
17. K. Peithmann, N. Korneev, M. Flaspöhler, K. Buse, and E. Krätzig, Rapid research notes, see phys.stat.sol (a) 178 (2000), R1.
18. K. Buse, Appl Phys B 64 (1997), 391.
19. K. Jermann and E. Krätzig, Appl Phys A 55 (1992), 114.
20. Y. Furukawa, M. Sato, K. Kitamura, Y. Yajima, and M. Minakata, J Appl Phys 72 (1992), 3250.
21. J.K. Yamamoto, K. Kitamura, N. Iyi, S. Kimura, Y. Furukawa, and M. Sato, Appl Phys Lett 61 (1992), 2156.
22. A. Adibi, K. Buse, and D. Psaltis, Appl Opt 40 (2001), 5175.
23. T. Volk, B. Maximov, S. Sulyanov, N. Rubinina, and M. Wöhlecke, Opt Mater 23 (2003), 229.

THEORETICAL INVESTIGATION OF METALLIC ELLIPTICALLY PERIODIC STRUCTURES USING MATHIEU FUNCTIONS

T. A. Denidni and H. Boutayeb
INRS-EMT
800 rue de la Gauchetiere
Montréal Québec H5A 1K6, Canada

Received 15 November 2005

ABSTRACT: *In this paper, an analysis of elliptical periodic structures composed of metallic wires is presented. The transmission and reflection coefficients of elliptical frequency-selective surfaces (FSSs) are calculated by expressing the scattered field via Mathieu functions and by using an elliptical-wave multiple reflections model. It is shown that when the elliptical period and the focus are constant, elliptical periodic surfaces have the same transmission and reflection coefficients. This work has potential applications for designing directive antennas.* © 2006 Wiley Periodicals, Inc. Microwave Opt Technol Lett 48: 988–992, 2006; Published online in Wiley InterScience (www.interscience.wiley.com). DOI 10.1002/mop.21543

Key words: *periodic structures; EBG structures; elliptical structures; Mathieu functions*

1. INTRODUCTION

Recently, a new directive antenna incorporating an elliptical electromagnetic band gap (EEBG) structure was designed, fabricated, and tested [1]. However, this structure has not been sufficiently studied; only experimental investigations have been presented. In this paper, a theoretical analysis of elliptical periodic structures excited by elliptical waves from their inside is proposed.

In [2, 3], a method was proposed for extracting the reflection and transmission coefficients of a cylindrical frequency-selective surface (FSS), and the obtained results were validated using a full-wave method. The method has been based on the multiple reflection between the cylindrical FSS and its center. In addition, compared to cylindrical EBG structures, elliptical EBG structures are more compact. Furthermore, antennas based on these structures conserve a large frequency bandwidth [1].

This paper proposes an analysis of elliptical periodic structures excited in their inside by elliptical waves. A multiple-reflection wave model is developed in order to be generalized to elliptical structures. First, the analysis that has been carried out for cylindrical EBG structures [2, 3] is used and then, because of the elliptical geometry of the studied structures, Mathieu functions are employed [4, 5].

To address this issue, elliptic coordinates have been considered in many electromagnetic problems [6–14]. In [6, 7], the scattering for a plane incident wave by infinite long multilayer elliptical cylinders has been studied, whereas in [8], the author considered a semi-elliptical cavity. In addition, an elliptical waveguide was analyzed in [9], the radiation of a slot elliptical antenna was described in [10], and an elliptical microstrip antenna was studied in [11]. Fast computation methods for elliptical waves have been also proposed [12, 13]. However, to our knowledge, the interactions between electromagnetic waves and elliptically periodic structures have not been studied yet.

The notation of the Mathieu functions varies considerably in the literature, and this paper follows the notation used in [13]. The analysis procedure for elliptical periodic structures excited by elliptical waves is presented in the following sections. In section 2,